Dynamic analysis of pathogen-infected host cells using quantitative phase microscopy

Seungrag Lee
Young Ran Kim
Ji Yong Lee
Joon Haeng Rhee
Chang-Soo Park
Dug Young Kim

Dynamic analysis of pathogen-infected host cells using quantitative phase microscopy

Seungrag Lee,[a] Young Ran Kim,[b] Ji Yong Lee,[a] Joon Haeng Rhee,[c] Chang-Soo Park,[a] and Dug Young Kim[d]
[a]Gwangju Institute of Science and Technology, Department of Information and Communications, 1 Oryong-dong, Buk-gu, Gwangju, 500–712 Republic of Korea
[b]Dongshin University, Department of Oriental Medicine Materials, 252 Daeho-dong, Naju, Jeonnam, 520–714 Republic of Korea
[c]Chonnam National University Medical School, Clinical Vaccine R&D Center, Research Institute of Vibrio Infection and Genome Research Center for Enteropathogenic Bacteria, Republic of Korea
[d]Yonsei University, Department of Physics, 262 Seongsanno, Seodaemun-gu, Seoul, 120–749 Republic of Korea

Abstract. We present the real-time quantitative analysis of *Vibrio vulnificus*–infected host cells using quantitative phase microscopy (QPM) based on interferometric techniques. This provides the ability to retrieve the phase or optical path-length distribution over the cell with nanometer path-length sensitivity from a single interferogram image. We have used QPM to study dynamic cell morphologic changes and to noninvasively quantify the cell volumes of rat basophilic leukemia RBL-2H3 cells infected with *V. vulnificus* strains: wild type (MO6–24/O) and RtxA1 toxin mutant (CMM770). During the process of *V. vulnificus* infection in RBL-2H3 cells, the dynamic changes of quantitative phase images, cell volumes, and areas were observed in real time using QPM. In contrast, dramatic changes were not detected in RBL-2H3 cells infected with the noncytotoxic RtxA1 toxin mutant. The results showed good correlation between QPM analysis and biochemical assays, such as lactate dehydrogenase assay or β-hexosaminidase release assay. We suggest that QPM is a powerful quantitative method to study the dynamic process of host cells infected with pathogens in a noninvasive manner. © *2011 Society of Photo-Optical Instrumentation Engineers (SPIE).* [DOI: 10.1117/1.3548882]

1 Introduction

Conventional optical imaging techniques such as phase-contrast microscopy and differential interference contrast microscopy (DICM) cannot commonly provide the actual thickness of a sample because factors such as baseline pixel intensity varied from one cell to the next. Lately, there are some proposed noble DICM schemes to retrieve the quantitative phase from DICM data,[1] with the extra cost of complicated computational procedures. Quantitative phase microscopy (QPM) is a powerful method to retrieve the morphological information of a sample, where the thickness or the optical path length of an object is obtained quantitatively from an interference image. This method can provide information on the cell structure and dynamics with nanometer path-length sensitivity. The image acquisition rate depends only on the frame rate of a charge coupled device (CCD) used in a QPM setup. Various QPM techniques for noninvasive and quantitative analysis of live cells have been developed over the past several years, such as Fourier phase microscopy,[2, 3] Hilbert phase microscopy,[4] diffraction phase microscopy,[5, 6] digital holographic microscopy,[7–9] and heterodyne Mach-Zehnder phase microscopy.[10] These techniques demonstrated the ability to measure not only the quantitative information of red blood cell (RBC) shapes and dynamics but also the spatial and temporal behavior of RBC membrane fluctuations. Furthermore, QPM has recently emerged as a powerful quantitative analysis for evaluating complex dynamic phenomena such as cell growth,[11] cycle,[12] and motility.[13–15] We have proposed and demonstrated QPM with autofocusing and edge-detection techniques for accurate cell volume measurement,[16] where autofocusing was applied to find the focus position of a sample, and edge detection was also used to accurately resolve the boundary between a cell and its suspension medium. QPM allows us to retrieve the phase or optical path-length distribution over a two-dimensional cell surface from a single interferogram image, where the optical path length can be obtained with nanometer sensitivity.

In this paper, we have shown that QPM with nanometer path-length sensitivity can be effectively used to study the dynamic properties of host-pathogen interactions and to monitor the detailed process of bacterial infection of a host cell. *Vibrio vulnificus* is used as a model organism of pathogenic bacteria in our study because this pathogen causes acute cytotoxicity to various host cells and manifests a wide *in vivo* pathologic spectrum that could cover most virulent bacterial infections from microscopic cell death to intractable septic shock.[17–19] We have previously reported that a proteinceous exotoxin of *V. vulnificus* called RtxA1 toxin causes host cell rounding and blebbing of the plasma membrane only when it is allowed to contact

Address all correspondence to: Young Ran Kim, Dongshin University, Department of Oriental Medicine Materials, 252 Daeho-dong, Naju, Jeonnam, 520–714 Republic of Korea. Tel: +82–61-330–3262; Fax: +82–61-379–7895; E-mail: kimyr@dsu.ac.kr and Joon Haeng Rhee, MD, Chonnam National University Medical School, Clinical Vaccine R&D Center and Department of Microbiology, 5 Hak-Dong, Dong-Ku, Gwangju, 501-746, Republic of Korea. Tel: +82–613797891; Fax: +82–613797895; E-mail: jhrhee@chonnam.ac.kr.
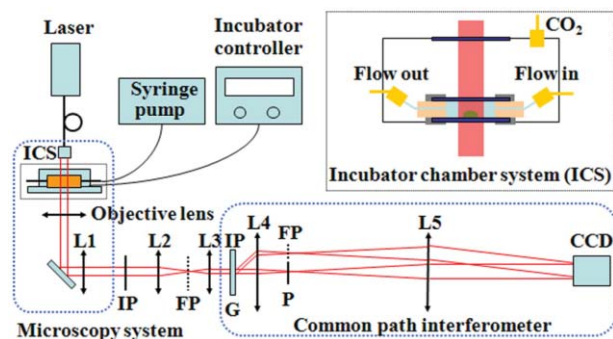
Fig. 1 Experimental setup of QPM for the examination of a live cell. Inset is incubator chamber system.

host cells.[19] Through previous observations of host–*V. vulnificus* interactions with light and confocal microscopy, we have an impression that infected host cells underwent a significant volume change. We suspect that these volume variations are essential characteristics of infected cells resulting from biochemical interactions between host cells and infecting pathogens. The accurate and real-time measurement of volume and morphologic changes will certainly provide new information concerning many host-pathogen interactions. We demonstrate dynamic analysis of *V. vulnificus* infection in RBL-2H3 cells in real time using QPM; we monitored the dynamic morphological changes, such as the volume and the surface area of an RBL-2H3 cell infected with wild-type (MO6–24/O) or RtxA1 toxin mutant (*rtxA1-*). In the present study, we tested whether the morphological changes in the infected cells measured by the QPM correlated with conventional biochemical analysis, such as cytotoxicity assay or β-hexosaminidase release assay.

2 Materials and Methods

2.1 Cell Culture

Rat basophilic leukemia RBL-2H3 (ATCC Company, Manassas, Virginia) cells were grown in minimal essential medium (MEM) with Earle's salt supplemented with 10% fetal bovine serum (FBS) and 2% L-glutamine (all from GIBCO Invitrogen, Carlsbad, California), in an incubator with a humidified atmosphere (5% CO_2) at 37°C. We used this cell line because it releases granules containing β-hexosaminidase when exogenously stimulated and consequently will have smaller volume after degranulation.

2.2 Bacterial Strains

MO6–24/O is a clinical isolate of *V. vulnificus*, and CMM770 (*rtxA1-*) is MO6–24/O with a deletion mutation in *rtxA1* gene.[19] *V. vulnificus* strains inoculated in 2.5% NaCl heat infusion broth were grown in a 37°C shaking incubator at 200 rpm.

2.3 Experimental Setup of QPM and Sample Preparation

The experimental setup of our QPM is based on the common path diffraction phase microscopy setup initially proposed by Popescu et al.[5] and is shown in Fig. 1. The setup is designed for quantitative phase imaging of a transparent sample. The basic configuration is a common path interferometer utilizing an inverted microscopy system with a live cell incubator system (CIS) and a CCD. A laser diode was used as an optical source with a center wavelength of 633 nm. A sample was imaged on the image plane (IP) through a 10× objective lens with 0.25 numerical aperture and another lens 1 (L1) with a 180-mm focal length. Optical magnification of the object on the IP1 was about 20. The focal lengths of the L2 and L3 lenses were 50 and 50 mm, respectively. L2 and L3 formed a 4f system to adjust the total magnification of our QPM system. A 110-grooves/mm transmission grating (G) was used to split a laser beam in two. We made a common path interferometer with only the zeroth- and first-order diffraction beams. The high-frequency information of the zeroth-order beam was filtered with a pinhole (P), and it served as a reference beam. The focal lengths of the L4 and L5 lenses were 100 and 500 mm, respectively. The L4 lens combined with the L5 lens formed another 4f system with five times the magnification. The filtered beam and the first-order diffracted beam were combined to form an interference pattern on the CCD plane. The optical magnification of the sample on the CCD plane was calibrated to be about 50. One period of a sinusoidal interference was sampled with 6 pixels in our CCD for both the *x*- and *y*-axes. The live cell incubator system consists of an incubator controller and a modified incubator chamber to allow continuous flow input from a syringe pump. The structure of the CIS is depicted in the dashed box of Fig. 1. A CCD (IPX-VGA210-L, Imperx Inc.) was used to acquire interference images. The CCD has an image acquisition rate of 200 fps at a full resolution of 640×480 pixels. The pixel-to-pixel distance of the CCD is 7.4 μm.

RBL-2H3 cells were seeded on a cover glass at a density of 1×10^5 cells/well and cultured overnight. The cells were washed two times with MEM and then sealed tightly in a special chamber filled with MEM. *V. vulnificus* wild-type strain cells were injected into the chamber within 10 s with a syringe pump (KDScientific, Holliston, Massachusetts), and images were captured every 10 s for 90 min. The same processes were performed with the RtxA1 toxin mutant strain (CMM770) by replacing the *V. vulnificus* wild-type strain (MO6–24/O).

2.4 Cell Images

Live cell images were obtained from RBL-2H3 cells infected with *V. vulnificus* strains in an eight-well chambered cover glass with cover No. 1 German borosilicate (Nalge Nunc International, Rochester, New York). RBL-2H3 cells were seeded at a density of 3×10^4 cells/well in MEM with 10% FBS and cultured overnight. The cells were washed with serum-free MEM medium, and each *V. vulnificus* strain was added at a multiplicity of infection (MOI) of 100. Cell images were acquired by DICM with a digital camera (Nikon).

2.5 Biochemical Analysis of V. vulnificus Cytotoxicity to RBL-2H3 Cells

RBL-2H3 cells were seeded at a density of 5×10^4 cells/well in a 48-well tissue culture plate (Corning, New York, New York) and cultured overnight. The cells were washed with serum-free MEM medium and infected with *V. vulnificus* at an MOI of 100. The culture supernatant (50 μl) was removed and
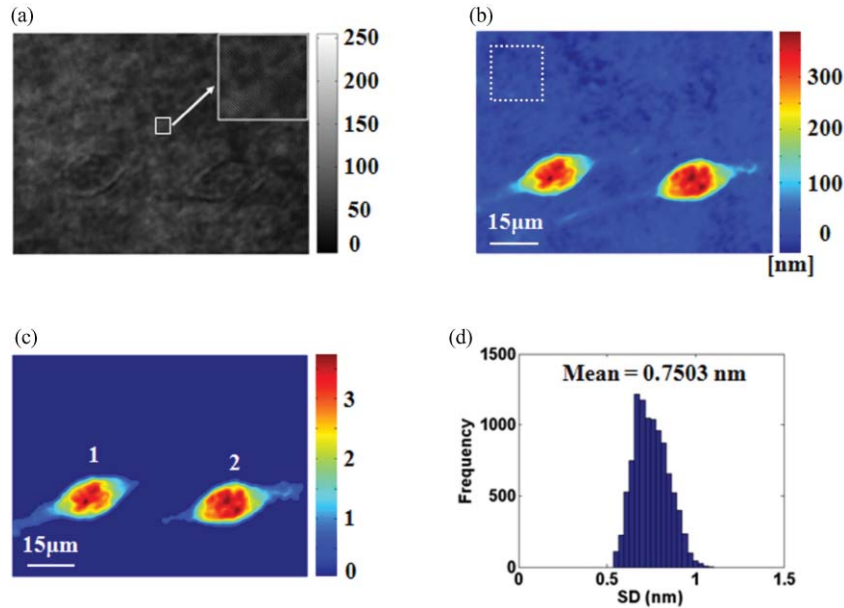
Fig. 2 Quantitative phase imaging and system stability of QPM. (a) The interferogram image of RBL-2H3 cells. Inset is the expanded interferogram image of the small square region. (b) The quantitative phase image of (a). The color bar indicates the optical path length in nanometers. (c) The edge-detected phase image of (b). The color bars indicate the phase in radians. (d) The histogram of SD in a series of optical path-length fluctuations at a point within the white dashed box in (b). The size of white dashed box is 100×100 pixels.

centrifuged for 1 min at 10,000 rpm. Lactate hehydrogrnase (LDH) released in the supernatant was assayed using the CytoTox96™ nonradioactive cytotoxicity assay kit (Promega, Madison, Wisconsin) in accordance with the manufacturer's protocol.[19]

Degranulation from RBL-2H3 cells was measured by determining the enzymatic activity of β-hexosaminidase in the supernatant. The supernatant from RBL-2H3 cells treated with *V. vulnificus* strains was transferred to a 96-well plate (30 μl/well), and 50 μl of 4-nitropheny1 *N*-acety1-β-D-glucosaminide (1.3 mg/ml in 0.1 M citric acid buffer pH 4.5) was added. After 1 h of incubation at 37°C, 100 μl of stop solution (0.1 M Na_2CO_3, $NaHCO_3$) was added and the absorbance was measured at 405 nm. The total content of β-hexosaminidase was quantified by lysing the cells with 1% Triton X-100.

2.6 Statistical Analysis

All values are expected as means $\pm$ standard error of the mean. Statistical comparisons were made using Student's t-test. Experiments were repeated three or four times and results from a representative experiment are shown.

3 Results and Discussion

3.1 Quantitative Real-Time Analysis Using QPM

To demonstrate the effectiveness of quantitative real-time analysis using QPM, we have measured the volume and the projected area of a single live RBL-2H3 cell for 90 min, including the measurement error of the optical path length in a series of phase images. RBL-2H3 cells seeded on a cover glass were sealed in a chamber filled with MEM.

We captured the quantitative phase image of RBL-2H3 cells in a focus position with the QPM system. The interferogram image of RBL-2H3 cells and its quantitative phase image are shown in Figs. 2(a) and 2(b) where the color bar indicates the optical path length in nanometers. We have applied an edge-detection technique to find the boundary between a cell and its surrounding medium before calculating the volume of a cell.[16] Figure 2(c) shows the edge-detected phase image of Fig. 2(b), where the fluctuation phase of surrounding background around the RBL-2H3 cells is forced to be zero and the color bar indicates the phase in radians. Figure 2(d) illustrates the system stability of our QPM setup. The measured thickness of empty volume without a sample should be zero in theory. However, its measured value does not become zero due to the noises of our measurement system such as vibration in optical components, liquid flow in a sample chamber, or air turbulence in the reference arm of an interferometer. We have used it as a parameter to tell the stability of our cell volume measurement. The system stability of our QPM setup was defined as the standard deviation (SD) of repeated optical path-length measurements at a point in a series of phase images within a white square of 100×100 pixels in Fig. 2(b), where there is no sample cell. Figure 2(d) shows the histogram of SD in a series of OPLF for 90 min. Phase images were taken every 10 s for 90 min by the QPM. The averaged value of SD was 0.7503 nm in Fig. 2(d), which demonstrates subnanometer stability in the path-length measurement of a cell thickness.

Using this QPM setup, the volume and projected area of RBL-2H3 cells were monitored for ∼90 min. Figures 3(a) and 3(b) show the volume and the projected area of RBL-2H3 cells indicated by the numbers 1 and 2 in Fig. 2(c). The quantitative phase image of Fig. 2(c) could be easily converted into a 2-D thickness image by applying the certain refractive indexes of an RBL-2H3 cell and the surrounding medium, where the refractive indexes of an RBL-2H3 cell and the surrounding medium were reported to be 1.40 and 1.33, respectively.[20] The cell volume
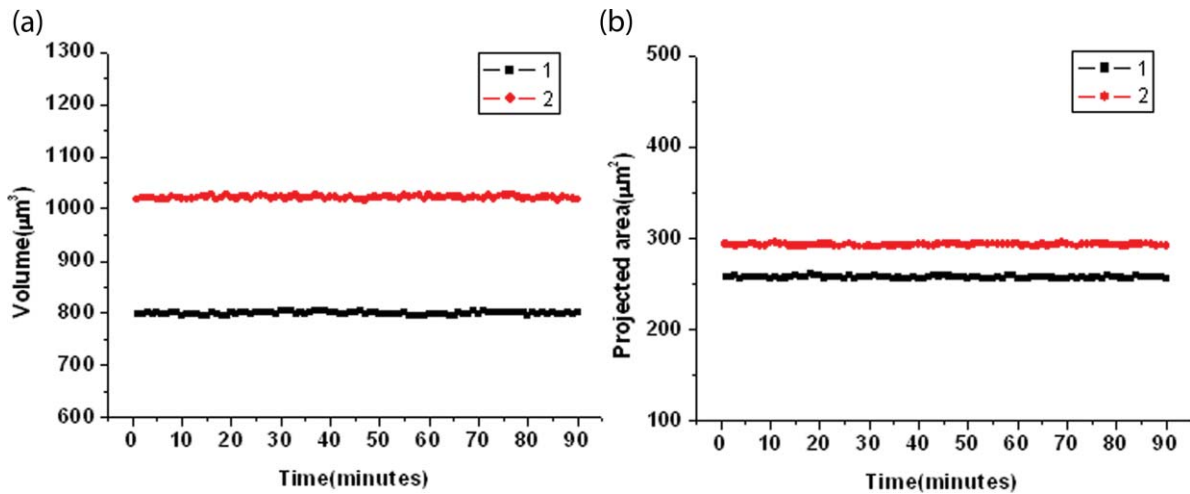
Fig. 3 Quantitative real-time analysis of a single live cell using QPM. (a) The measured volumes of an RBL-2H3 cell from Fig. 2(c). (b) The projected area of an RBL-2H3 cell over 90 min.

was calculated by the sum of the thicknesses within the cell boundary in Fig. 2(c). During the measurement, the volume and the projected area of an RBL-2H3 cell were kept constant by filling the chamber with MEM without FBS supplementation. These results demonstrate usefulness of the quantitative real-time analysis applied to measure the dynamics of a live cell for 90 min.

### 3.2 Dynamic Analysis of Bacterial Infection in RBL-2H3 Cells

To analyze the dynamic changes of RBL-2H3 cells infected with cytotoxic *V. vulnificus*, we observed quantitative phase image changes and measured the volume and projected area of each infected cell using the analysis method mentioned in Sec. 3.1. RBL-2H3 cells were infected with wild-type *V. vulnificus* at an MOI of 100 for 90 min.

Figures 4(a) and 4(b) show the quantitative phase images of RBL-2H3 cells and the pseudo 3-D phase image at the first measurement using QPM. As shown in Fig. 4(c), the edge-detected phase image indicated by the white dashed square in Fig. 4(a) was obtained to calculate more accurate cell volume and projected area using the edge-detection imaging technique,[16] where color bars indicate the phase in radians.

Figure 5 shows quantitative phase images of an RBL-2H3 cell at different time points during the first 90 min. Note that the RtxA1 toxin of *V. vulnificus* induces cytoskeletal rearrangements and plasma membrane blebs only when *V. vulnificus* is allowed to contact host cells.[19] The results obtained from Fig. 5 illustrate the process of contact cytotoxicity between *V. vulnificus* and host cells, where the color bar represents the phase in radians. During the first 20 min, the shape of a cell became rounded and the rounded cell shape did not change much until 48 min. The cell rounding was supposed to be the result of actin aggregation
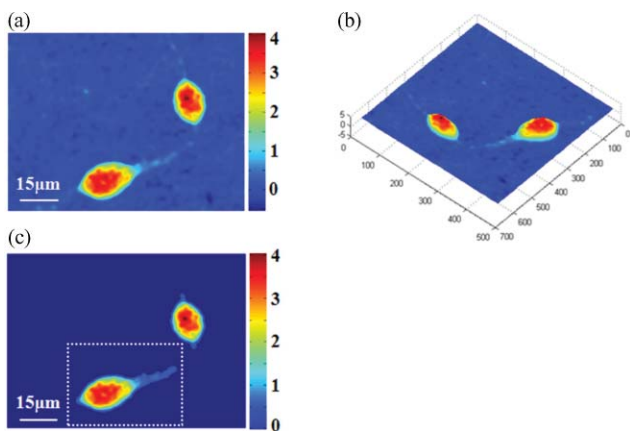
Fig. 4 Quantitative phase imaging at the first measurement for dynamic analysis of *V. vulnificus*–infected RBL-2H3 cell. (a) The quantitative phase image of RBL-2H3 cells. (b) The pseudo 3-D phase image of (a). (c) The edge-detected phase image indicated by the arrow in (a). The color bars indicate the phase in radians.
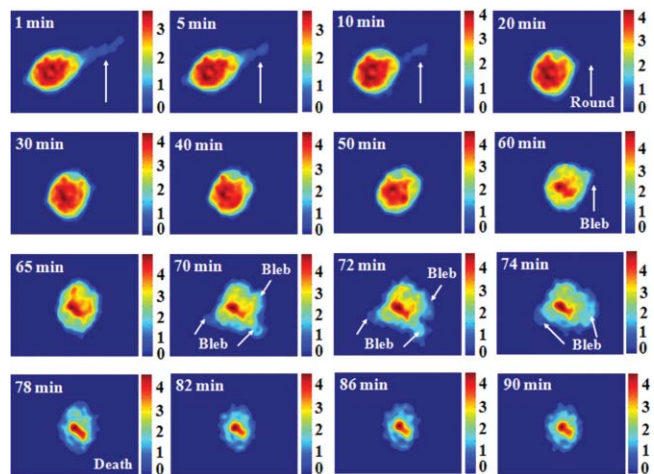
Fig. 5 RtxA1 toxin of *V. vulnificus* induces cytoskeletal rearrangements and plasma membrane blebs only when *V. vulnificus* is allowed to contact host cells. The quantitative phase images of an RBL-2H3 cell injected by *V. vulnificus* at different time points during the first 90 min. The color bars indicate the phase in radians.
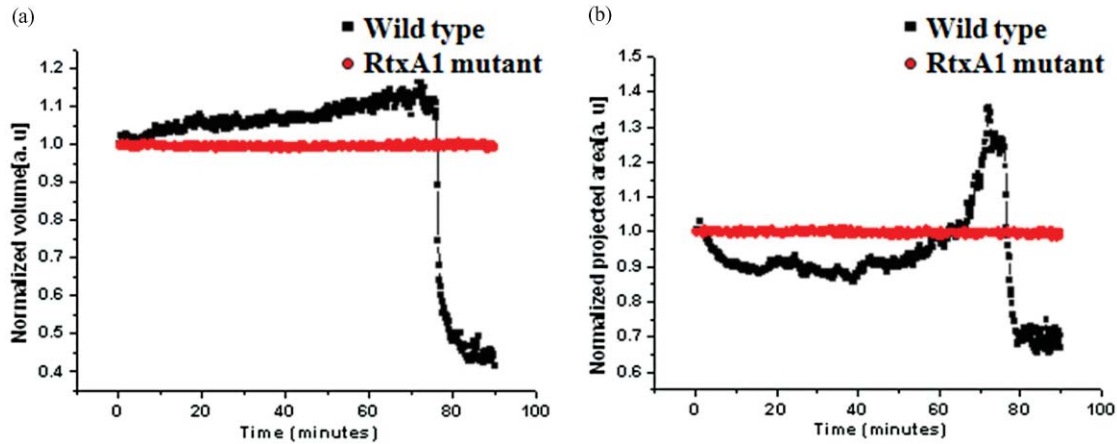
Fig. 6 Pathogenic role of RtxA1 toxin in the killing and cell volume change in host cells. (a) The dynamic changes of the volume and projected area in a RBL-2H3 cell infected with *V. vulnificus* strains. (b) The dynamic changes of the projected area. To compare differences between wild type and mutant, the volume and projected areas were normalized by setting the initial cell volume and projected area as 1.0. Black squares and red dots display wild type and RtxA1 mutant type, respectively.

induced by RtxA1.[19] The cytoplasmic membrane blebbing was observed from approximately 48 to 76 min. After 76 min, the RBL-2H3 cell appeared to be burst to death, leaving only ghost cell remnants.

To quantitatively visualize the pathogen-induced host cell death process, the volume and the projected area of RBL-2H3 cells infected with *V. vulnificus* wild-type and RtxA1 toxin mutant type were measured every 10 s for 90 min. To compare differences between wild-type and mutant, the volumes and projected areas were normalized by setting the initial cell volume and projected area as 1.0 (Fig. 6). The cell volume of the wild-type *V. vulnificus*–infected RBL-2H3 cell [Fig. 6(a), black dots] remained roughly stable or minutely increased for the first 48 min. This period corresponds to the period when the cell rounding was maintained in Fig. 5. From 48 to 76 min, the volume of the wild-type *V. vulnificus*–infected RBL-2H3 cell increased slightly and more projected area fluctuations were noted. These findings should have resulted from the water influx through micropores formed in the host cell affected by the RtxA1 toxin.[19] Starting at ∼76 min, the cell volume of the wild-type *V. vulnificus*–infected RBL-2H3 cell showed a sharp decline and did not recover. This was presumably due to an irreversible death of the cell. Black dots in Fig. 6(b) showed that the projected area of the wild-type *V. vulnificus*–infected RBL-2H3 cell slightly decreased during the cell rounding period while the cell volume did not decrease. This finding suggests that wild-type *V. vulnificus* infection-induced actin aggregation causes elevation of cell height and regression of cell margin. Starting from 48 min, the projected area of the wild-type *V. vulnificus*–infected RBL-2H3 cell increased significantly and reached a peak at 72 min] Fig. 6(b), black dots]. This might be due to the membrane blebbing of the cell. The dramatic drop in the cell area was observed from 76 to 79 min, and the cell area did not recover afterward because of the cell burst. Our dynamic analysis has demonstrated that the host cell infected with wild-type *V. vulnificus* at an MOI of 100 had been killed irreversibly after 72 min by cell burst.

To observe the pathogenic role of RtxA1 toxin in the killing and cell volume change in host cells, an *rtxA1* gene-deletion

mutant was incubated with RBL-2H3 cells at an MOI of 100 for 90 min. Unlike the case of wild-type *V. vulnificus*, no significant changes in cell volumes and projected area were observed with QPM in RBL-2H3 cells incubated with the RtxA1 toxin mutant [Figs. 6(a) and 6(b) red dots]. No host cell rounding and blebbing of plasma membrane were observed in the case of mutant-type *V. vulnificus* as shown in Fig. 7. The present results are quite consistent with those we had obtained before with *rtxA1* deletion mutant using confocal microscopy.[19]

Immediately before the cell burst, in the wild-type *V. vulnificus*–infected cells, cell volume and projected area increased by 15 and 35%, respectively. The projected cell area decreased by 10% until the start of membrane blebbing. Since projected area change is evident as early as 10 min after infection, even a very small amount of RtxA1 toxin transferred to host cells seems to trigger actin rearrangement. In this regard, we expect that the QPM will provide more detailed and dynamic information about host-parasite interactions, which is difficult by conventional microscopy and still image analyses.
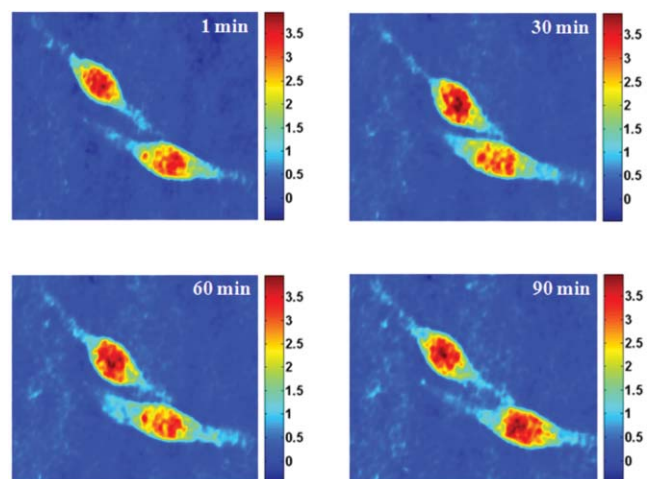
Fig. 7 *V. vulnificus* mutant type (CMM770) infection to RBL-2H3 cells for 90 min.
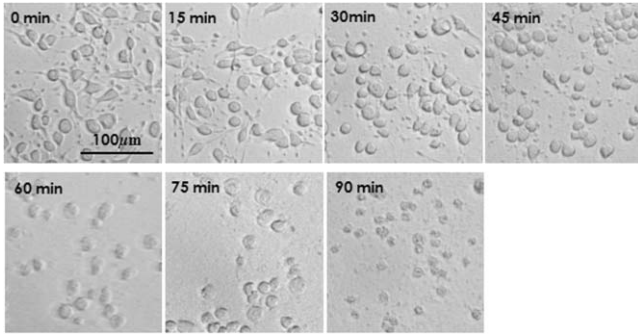
Fig. 8 Dynamic changes of *V. vulnificus*–infected RBL-2H3 cells using DICM. Dynamic morphologic changes of RBL-2H3 cells infected with *V. vulnificus* were displayed with images captured by a conventional DIC microscope.

3.3 Correlation among Information Obtained by QPM and Conventional Assays

Live *V. vulnificus* is highly cytotoxic to host cells *in vivo* and *in vitro*, and the cytotoxicity has been regarded as the hallmark of the pathogenicity of the microorganism.[19] Figure 8 displays still photos showing morphologic changes of RBL-2H3 cells infected with wild-type *V. vulnificus*. As can be seen in these images, it is hard to deduce quantitative parameters that can characterize the condition of a cell. Significant cell rounding can be observed from 30 min. The cell size seemed to decrease in a time-dependent manner. The RBL-2H3 cells infected with the wild-type *V. vulnificus* showed almost synchronized responses. On the basis of this finding, we could assume that biochemical assays for population cell death could be correlated with single-cell QPM analysis. However, it is almost impossible to quantitatively monitor biological changes in the infected host cells using only the microscopic still images.

Death of a given cell population could be dynamically monitored by a time course assay of cytoplasmic proteins that were released from dying cells to the supernatant. LDH is a cytosolic enzyme universally present in eukaryotic cells and exerts enzyme activities as tetramers with approximate molecular mass of 142,000.[21] The enzyme comes out from dying cells through the damaged plasma membrane. We have quantified the cytotoxic activity of *V. vulnificus* by measuring the amount of LDH released from dying RBL-2H3 cells. Significant LDH release could be observed from 45 min in Fig. 9(a). This means that plasma membrane damage allowing exit of the macromolecular LDH was established after 45 min. On the other hand, QPM depicted host cell change as early as 10 min and suggested an abrupt change in the plasma membrane structure around 48 min, which allowed more water influx, resulting in a significant cell volume increase. The time difference between the two measurements (LDH release assay and QPM) might have originated from the different culture conditions. In the QPM experiments, the pathogen-host cell interaction was observed in a concealed container, whereas the LDH release assay was performed in a conventional culture condition. As reported elsewhere,[19] the *rtxA1* mutant did not cause LDH release until 90 min.

We also assayed β-hexosaminidase release from *V. vulnificus*–treated RBL-2H3 cells, a marker of the degranulation of the cells as shown in Fig. 9(b). Since β-hexosaminidase is confined in the basophilic granules in the RBL-2H3 cells, release of the enzyme to the supernatant means the membrane damage is big enough to allow degranulation. The membrane damage should exceed the secretory granule sizes between 0.4 and 0.8 μm^2.[22] A significant increase in the β-hexosaminidase release approximately coincided with an abrupt decrease in cell volume and projected area (the cell burst time point). Taken together, our QPM analysis results are well correlated with conventional biochemical and morphological assay methods, and
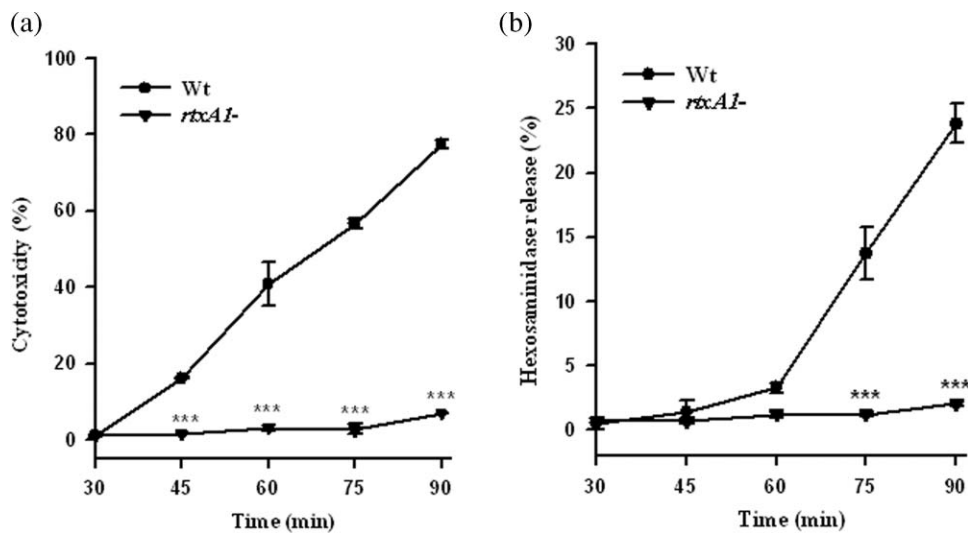
Fig. 9 Identification of *rtxA1* gene causing time-dependent cell death using biochemicals. (a) *V. vulnificus* cytotoxicity to RBL-2H3 cells. *V. vulnificus* cells were treated to RBL-2H3 cells at an MOI 100 for 90 min. LDH released in supernatant was assayed as a marker of the cytotoxicity. (b) Hexosaminidase release assay. Degranulation from RBL-2H3 cells was measured by determining the enzymatic activity of β-hexosaminidase in the supernatant (*** $P < 0.001$).

could recognize subtle changes from far earlier stages of the host-pathogen interaction.

4 Conclusion

We have demonstrated a practical application for QPM in studying the real-time dynamics of host-pathogen interactions in a single cell in a noninvasive manner. By measuring the changes in the volume and the projected area of a cell with QPM, it was shown that dynamic changes in the process of *V. vulnificus* infection of an RBL-2H3 cell could be effectively monitored. We have verified that the pathogenic significance of the *V. vulnificus rtxA1* gene can be effectively quantified by measuring the volume or projected area of an RBL-2H3 cell infected with wild-type (MO6–24/O) or mutant (*rtxA1-*) *V. vulnificus*. We have also shown that the QPM results correlated well with the LDH and β-hexosaminidase release from dying cells. Because it was proved that accurate quantitative real-time measurement for the volume or the projected area of a cell is practicable by our proposed method, we anticipate that our QPM technique will be a powerful and practical tool for studying the rapid quantitative characterization of host-pathogen interactions and other cell biological mechanisms.

References

1. B. Kouskousis, D. J. Kitcher, S. Collins, A. Roberts, and G. W. Baxter, "Quantitative phase and refractive index analysis of optical fibers using differential interference contrast microscopy," *Appl. Opt.* **47**, 5182–5189 (2008).
2. G. Popescu, L. P. Deflores, J. C. Vaughan, K. Badizadegan, H. Iwai, R. R. Dasari, and M. S. Feld, "Fourier phase microscopy for investigation of biological structures and dynamics," *Opt. Lett.* **29**, 2503–2505 (2004).
3. N. Lue, W. S. Choi, G. Popescu, T. Ikeda, R. R. Dasari, K. Badizadegan, and M. S. Feld, "Quantitative phase imaging of live cells using fast Fourier phase microscopy," *Appl. Opt.* **46**, 1836–1842 (2007).
4. T. Ikeda, G. Popescu, R. R. Dasari, and M. S. Feld, "Hilbert phase microscopy for investigating fast dynamics in transparent systems," *Opt. Lett.* **30**, 1165–1168 (2005).
5. G. Popescu, T. Ikeda, R. R. Dasari, and M. S. Feld, "Diffraction phase microscopy for quantifying cell structure and dynamics," *Opt. Lett.* **31**, 775–777 (2006).
6. Y. Park, G. Popescu, K. Badizadegan, R. R. Dasari, and M. S. Feld, "Diffraction phase and fluorescence microscopy," *Opt. Express* **14**, 8263–8268 (2006).
7. B. Rappaz, P. Marquet, E. Cuche, Y. Emery, C. Depeursinge, and P. Magistretti, "Measurement of the integral refractive index and dynamic cell morphometry of living cells with digital holographic microscopy," *Opt. Express* **13**, 9361–9373 (2005).
8. P. Marquet, B. Rappaz, P. J. Magistretti, E. Cuche, Y. Emery, T. Colomb, and C. Depeursinge, "Digital holographic microscopy: A noninvasive contrast imaging technique allowing quantitative visualization of living cells with subwavelength axial accuracy," *Opt. Lett.* **30**, 468–470 (2005).
9. B. Rappaz, B. Alexander, Y. Emery, R. Korenstein, C. Depeursinge, P. J. Magistretti, and P. Marquet, "Comparative study of human erythrocytes by digital holographic microscopy, confocal microscopy, and impedence volume analyzer," *Cytometry Part A* **73A**, 895–903 (2008).
10. C. Fang-Yen, S. Oh, Y. Park, W. Choi, S. Song, H. S. Seung, R. R. Dasari, and M. S. Feld, "Imaging voltage-dependent cell motions with heterodyne Mach–Zehnder phase microscopy," *Opt. Lett.* **32**, 1572–1574 (2007).
11. G. Popescu, Y. Park, N. Lue, C. A. Best-Popescu, L. Deflores, R. R. Dasari, M. S. Feld, and K. Badizadegan, "Optical imaging of cell mass and growth dynamics," *Am. J. Physiol.: Cell Physiol.* **295**, C538–C544 (2008).
12. B. Rappaz, E. Cano, T. Colomb, J. Kühn, C. Depeursinge, V. Simanis, P. J. Magistretti, and P. Marquet, "Noninvasive characterization of the fission yeast cell cycle by monitoring dry mass with digital holographic microscopy," *J. Biomed. Opt.* **14**, 034049 (2009).
13. G. Popescu, Y. Park, R. R. Dasari, K. Badizadegan, and M. S. Feld, "Coherence properties of red blood cell membrane motions," *Phys. Rev. E* **76**, 021902 (2007).
14. G. Popescu, Y. Park, W. Choi, R. R. Dasari, M. S. Feld, and K. Badizadegan, "Imaging red blood cell dynamics by quantitative phase microscopy," *Blood Cells Mol. Diseases* **41**, 10–16 (2008).
15. Y. Park, M. Diez-Silva, G. Popescu, G. Lykotrafitis, W. Choi, M. S. Feld, and S. Suresh, "Refractive index maps and membrane dynamics of human red blood cells parasitized by plasmodium falciparum," *Proc. Natl. Acad. Sci. U.S.A.* **105**, 13730 (2008).
16. S. Lee, J. Y. Lee, W. Z. Yang, and D. Y. Kim, "Autofocusing an edge detection schemes in cell volume measurements with quantitative phase microscopy," *Opt. Express* **17**, 6476–6486 (2009).
17. S. D. Park, H. S. Shon, and N. J. John, "*Vibrio vulnificus* septicemia in Korea: Clinical and epidemiological findings in 70 patients," *J. Am. Acad. Dermatol.* **24**, 397–403 (1991).
18. C. O. Tacket, F. Brenner, and P. A. Blake, "Clinical features and epidemiological study of *Vibrio vulnificus* infections," *J. Infect. Dis.* **149**, 559–561 (1984).
19. Y. R. Kim, S. E. Lee, H. Kook, J. A. Yeom, H. S. Na, S. Y. Kim, S. S. Chung, H. E. Choy, and J. H. Rhee, "*Vibrio vulnificus* RTX toxin kills host cells only after contact of the bacteria with host cells," *Cell. Microbiol.* **10**, 848–862 (2008).
20. W. Z. Yang, J. Y. Chen, J. T. Yu, and L. W. Zhou, "Effects of low power laser irradiation on intracellular calcium and histamine release in RBL-2H3 mast cells," *Photochem. Photobiol.* **83**, 979–984 (2007).
21. R. Jaeniche and S. Knofm, "Molecular weight and quaternary structure of lactic dehydrogenase: 3. comparative determination by sedimentation analysis, light scattering and osmosis," *Eur. J. Biochem.* **4**, 157–163 (1968).
22. E. Grimberg, Z. Peng, I. Hammel, and R. Sagi-Elsenberg, "Synaptotagmin III is a critical factor for the formation of the perinuclear endocytic recycling compartment and determination of secretory granules size," *J. Cell. Sci.* **116**(Pt 1), 145–154 (2003).